Journal of Computational Physics **174,** 552–578 (2001)
doi:10.1006/jcph.2001.6927, available online at http://www.idealibrary.com on IDEAL®

A Level-Set Method for Computing Solutions to Viscoelastic Two-Phase Flow

S. B. Pillapakkam and P. Singh

Department of Mechanical Engineering, New Jersey Institute of Technology, University Heights, Newark, New Jersey 07102
E-mail: sbp4124@njit.edu; singhp@njit.edu

Received May 2, 2000; revised July 10, 2001

A finite-element code based on the level-set method is developed for simulating the motion of viscoelastic two-phase flow problems. This method is a generalization of the finite-difference approach described in [1–4] for computing solutions to two-phase problems of inviscid and viscous fluids. The Marchuk–Yanenko operator-splitting technique is used to decouple the difficulties associated with the nonlinear convection term, the incompressibility constraint, the viscoelastic term, and the interface motion problem. The nonlinear convection problem is solved using a least-squares conjugate gradient algorithm, and the Stokes-like problem is solved using a conjugate gradient algorithm. The constitutive equation is solved using a scheme that guarantees the positive definiteness of the configuration tensor, while the convection term in the constitutive equation is discretized using a third-order upwinding scheme. The code is verified by performing a convergence study to show that the results are independent of the mesh and time-step sizes. Using our code we have studied the deformation of drops in simple shear and pressure-driven flows and of bubbles in gravity-driven flows over a wide range of dimensionless capillary (Ca) and Deborah numbers (De). For a Newtonian bubble rising in a quiescent viscoelastic liquid we find that there are limiting values of the parameters De and Ca, above which the bubble assumes a characteristic shape with a cusp-like trailing edge. The front of the bubble, however, remains round, as the local viscoelastic and viscous stresses act to round the bubble. In a pressure-driven flow the drop is stretched so that its front, which is closer to the channel center, remains round, and the trailing edge, which is closer to the channel wall, becomes sharp. These numerical results are in agreement with the experimental observations.

Key Words: viscoelastic fluids; Oldroyd-B fluid; level-set method; two-phase flows; drop deformation; operator-splitting.

0021-9991/01 $35.00

1. INTRODUCTION

A numerical method for simulating the motion of viscoelasitc two-phase flows is developed. The viscoelastic fluid is modeled via the Oldroyd-B model. This capability for direct numerical simulation of the two-phase flow problems of viscoelastic liquids could be useful in the modeling of many industrial processes.

For example, it is well known that immiscible polymer blends can be mixed by subjecting to shear flows. This happens naturally under some processing operations (e.g., extrusion), which improves the mechanical properties of the extruded products. One of the mechanisms that is believed to enhance mixing is the breakup of drops into smaller droplets under shear flows. The role of viscoelastic stresses in the breakup of drops, however, is not completely understood. This is at least partly due to the complexity of flow field, which makes the task of experimentally determining the distribution of viscoelastic stresses around the droplets very difficult, if not impossible. For numerical simulations, on the other hand, this is not a problem because the detailed velocity and stress distributions are known. The numerical approach therefore could be extremely valuable in explaining the role of viscoelastic stresses in the drop breakup as well as the physics of shear-induced mixing of polymer blends.

The problem of computing the motion of two-phase flows with interfaces is difficult even for Newtonian fluids because the interface shape changes in response to fluid motion. Across the interface the fluid properties change suddenly and an interfacial force acts along the interface of the two fluids. When one or both phases are viscoelastic, the numerical problem is even more complex, as one must also solve for the viscoelastic stresses.

There are several numerical approaches available for tracking the interface between two immiscible Newtonian liquids (e.g., the surface-tracking method [5], the volume-of-fluid method [6, 7], the mapping method [8], and the level-set method [1–4]). These methods have been used extensively to simulate viscous and inviscid two-phase flows. Due to the inherent complexity of viscoelastic flows, there are relatively fewer numerical schemes (e.g., the moving-grid method and the mapping method; see, respectively [9] and [10–12], and references therein). In this paper we use the level-set method to track the interface.

In the level-set method [1], the interface position is not explicitly tracked but is defined to be the zero level set of a smooth function ϕ, which is assumed to be the signed distance from the interface. In our implementation, it is assumed to be negative inside the drop surface and positive outside. Along the interface it is assumed to be zero. In order to track the interface, the level-set function is advected according to the velocity field. One of the attractive features of this approach is that it is relatively easy to implement in both two and three dimensions. In fact, an algorithm developed for two dimensions can be easily generalized to three dimensions. The level-set function can be represented using the same finite-element basis functions that are used for the velocity field. Also, the method does not require any special treatment when a front splits into two or when two fronts merge.

The finite-element scheme developed in this paper uses the Marchuk–Yanenko operator-splitting technique to decouple the difficulties associated with the incompressibility constraint, the nonlinear convection term, the interface motion, and the viscoelastic term [13–15]. The operator-splitting scheme gives rise to the following four subproblems: a Stokes-like problem for velocity and pressure, a nonlinear convection–diffusion problem for velocity, an advection problem for the configuration tensor, and an advection problem for the interface. The first problem is solved by using a conjugate gradient (CG) method [16] and the second problem is solved using a least-squares CG method [17]. The third

problem is a hyperbolic partial differential equation for the configuration tensor. The two key features of the numerical method used for solving this problem are a scheme that ensures the positive definiteness of the configuration tensor and a third-order upwinding scheme for discretizing the advection term in the constitutive equation [18]. These two features are important for obtaining a split scheme that is stable at relatively large Deborah (De) numbers. The fourth problem is for the advection of the level-set function ϕ, which is solved using a third-order upwinding scheme [19]. The advected ϕ is then reinitialized to be a distance function, which, as noted in [2], is essential for ensuring that the scheme accurately conserves mass. Also note that the linear systems in the Stokes-like and nonlinear problems are symmetric and hence can be solved by using the CG algorithm. In our code, the product of the global matrix and vectors, required in the CG algorithm, is computed directly without assembling the global matrix of the linear system. This reduces the memory requirement of the computer program.

We have used our code to investigate the dynamics of drop deformation in simple shear flows for the cases where the drop is Newtonian and the fluid is viscoelastic, and vice versa. In addition, we have investigated the deformation of a Newtonian drop in a viscoelastic pressure-driven flow and that of a rising bubble in a quiescent viscoelastic liquid. The drop (or bubble) is assumed to be immiscible with the bulk fluid. The code is verified by comparing the time-dependent velocity and configuration (stress) distributions for a drop subjected to a shear flow and for a rising bubble for three different mesh refinements, and for two different values of the time step.

A drop subjected to simple shear flow of strength G deforms under the influence of the flow-induced stresses on the surface, while the surface tension resists deformation. The parameters affecting deformation are the drop radius a, the interfacial tension γ, G, and the viscosity ratio $\lambda = \eta_L/\eta_d$, where η_L is the continuous phase viscosity and η_d is the viscosity of the fluid inside the drop. The parameters G, η_L, γ, and a can be combined to form a dimensionless group called the capillary number $\mathrm{Ca} = G\eta_L a/\gamma$. The Reynolds number $\mathrm{Re} = \rho G a^2/\eta_L$ determines the importance of inertial effects. The drop deformation when viscoelastic fluids are involved is relatively more complicated, as it is also a function of the Deborah number. The Deborah number $\mathrm{De} = \lambda_r G$ is a dimensionless measure of the viscoelastic stresses, where λ_r is the relaxation time of the fluid.

Numerical simulations are started by placing an initially circular drop of radius a in the flow. The drop deforms with time and, as in experiments, may or may not reach a steady state shape. Our calculations show that when there is a final steady state shape, it is a function of Ca and De. Similarly, the shape of a bubble rising in a viscoelastic liquid depends on both Ca and De.

For an elliptical drop, the deformation can be measured in terms of the deformation parameter D,

$$D = \frac{L - B}{L + B},$$

where L and B are, respectively, the major and minor axes of the ellipse. As we discuss later, in viscoelastic simple shear flows, the drops do not deform to elliptical shapes, and therefore strictly speaking, the measure D alone cannot completely quantify drop deformation. Another measure that quantifies the deviation from the elliptical shape is needed. But since our primary goal in this paper is to present the numerical method, we avoid this additional complication.

It is worth noting that experimental studies show that when the flow outside a drop or bubble is not axisymmetric, the deformed drop is also not axisymmetric [20]. For example, the deformed drop shape in simple shear flows is not axisymmetric. In fact, the deformed drop shape is not even symmetrical. When one or both of the liquids involved are viscoelastic, the drop asymmetry is greater, which, as discussed in Section 3, is due to the development of viscoelastic stress boundary layers near the interface that are not symmetrically located about the major axis of the deformed drop. Therefore, strictly speaking, for understanding the deformation and breakup of drops in viscoelastic simple shear flows, simulations must be performed in three dimensions.

Another problem we study is that of a bubble rising in a viscoelastic fluid. It was reported in [20] that a bubble rising in a viscoelastic liquid develops a two-dimensional cusp-like trailing edge when Ca is O(1), where $\mathrm{Ca} = U\eta_L a/\gamma$ and U is the velocity of the rising bubble. Specifically, the bubble appears to have a sharp cusp-like trailing edge in one view and a broad trailing edge in the orthogonal view. For capillary numbers below the critical value of O(1), the trailing edge of the bubble is round. The numerical simulations reported in [10] for an axisymmetric bubble are in agreement with these experimental observations, except that in experiments the cusp shape is two-dimensional. For our two-dimensional simulations, the bubble assumes a cusp-like trailing edge when Ca and De numbers are O(1), where $\mathrm{De} = \lambda_r U/(2a)$ and $2a$ is the diameter of the undeformed bubble.

The outline of the paper is as follows. In the next section we state the governing equations for the Oldroyd-B liquid, briefly describe the level-set approach, and present our finite-element method for viscoelastic two-phase flow. In Section 3, we discuss the convergence study that shows that the numerical results are independent of the mesh size as well as the time step. We also discuss the results for the deformation of drops in simple shear and pressure-driven flows of Newtonian and Oldroyd-B liquids, and for a bubble rising in an Oldroyd-B liquid.

2. GOVERNING EQUATIONS AND THE LEVEL-SET METHOD

The viscoelastic fluid in our simulations is modeled using the Oldroyd-B model. Most results presented in this paper are for two-dimensional flows. Let us denote the domain containing the viscoelastic fluid and a drop (or a bubble) by Ω, and the domain boundary by Γ. The upstream part of Γ is denoted by Γ^-. The governing equations for the two fluid system are

$$\nabla \cdot \mathbf{u} = 0, \tag{1}$$

$$\rho\left[\frac{\partial \mathbf{u}}{\partial t} + \mathbf{u}\cdot\nabla\mathbf{u}\right] = \rho\mathbf{g} - \nabla p + \nabla\cdot\left(\frac{c}{\lambda_r}\mathbf{A}\right) + \nabla\cdot(2\eta_s\mathbf{D}) + \gamma\kappa\delta(\phi)\mathbf{n}, \tag{2}$$

$$\mathbf{u} = \mathbf{u}_L \quad \text{on } \Gamma, \tag{3}$$

with the evolution of the configuration tensor $\mathbf{A}$ given by

$$\begin{aligned} &\frac{\partial \mathbf{A}}{\partial \mathbf{t}} + \mathbf{u}\cdot\nabla\mathbf{A} = \mathbf{A}\cdot\nabla\mathbf{u} + \nabla\mathbf{u}^T\cdot\mathbf{A} - \frac{1}{\lambda_r}(\mathbf{A}-\mathbf{I}), \\ &\mathbf{A} = \mathbf{A}_L \quad \text{on } \Gamma^-. \end{aligned} \tag{4}$$

Here $\mathbf{u}$ is the velocity, p is the pressure, η_s the solvent viscosity, ρ is the density, $\mathbf{D}$ is the symmetric part of the velocity gradient tensor, c is a measure of polymer concentration in terms of the zero shear viscosity, $\mathbf{n}$ is the outer normal, γ is the surface tension, κ is the surface curvature, ϕ is the distance from the interface, δ is the delta function, and λ_r is the relaxation time. The zero shear viscosity $\eta = \eta_s + \eta_p$, where $\eta_p = c\eta_s$, is the polymer contribution to viscosity. The fluid retardation time is equal to $\lambda_r/(1+c)$. The surface-tension force acts only along the interface where the level-set function ϕ is zero. Also note that in the Newtonian region, since the relaxation time is zero, from (4) $\mathbf{A} = \mathbf{I}$ and the viscoelastic stress term in (4) drops out because $\nabla \cdot \mathbf{A}$ is zero.

The level-set function ϕ is advected according to the local velocity; i.e.,

$$\frac{\partial \phi}{\partial t} + \mathbf{u} \cdot \nabla \phi = 0. \tag{5}$$

Clearly, if ϕ satisfies the above equation and $\phi = 0$ at $t = 0$ along the interface, the zero level set of ϕ marks the interface for all $t > 0$. When ϕ is advected according to (5) it will not remain the distance function for the points away from the interface, and therefore it must be reinitialized to be a distance function. But since only the zero level set is physically relevant, as noted in [21], "we have a lot of freedom in extending the level set function outside the interface." Later in this section, we discuss a finite-element scheme that can be used to reinitialize ϕ to be a distance function.

In the present method the governing equations are solved simultaneously everywhere (i.e., both inside and outside the drops/bubbles in the domain). In this sense our approach is different from the methods where the flow fields inside and outside the drop are decoupled and solved separately [11, 12]. In a decoupled approach one must apply suitable boundary conditions at the interface (i.e., impose the continuity of velocity and shear stress across the interface), and the jump in the normal stress across the interface is set to be equal to the surface-tension force. Since in our approach the governing equations are solved in a coupled manner, the method is stable and allows us to take relatively large time steps. It is worth noting that since we use an explicit scheme to advect the interface according to (5), the CFL criterion is pertinent to our calculations and thus when the time step is too large the numerical method fails.

2.1. *Reinitialization of ϕ*

The level-set function ϕ is reinitialized to be a distance function after each time step by solving to steady state the equation, obtained in [2],

$$\frac{\partial \phi}{\partial t} + \mathbf{w} \cdot \nabla \phi = S(\phi_0), \tag{6}$$

where ϕ_0 is the distribution to be reinitialized and

$$\mathbf{w} = S(\phi_0)\frac{\nabla \phi}{|\nabla \phi|}.$$

Here $S(\phi_0)$ is the sign function (i.e., $S(\phi_0) = 1$ if $\phi_0 > 0$ and $S(\phi_0) = -1$ if $\phi_0 < 0$). In order to avoid discontinuities, in our code we use the smoothed sign function

$$S(\phi_0) = \frac{\phi_0}{\sqrt{\phi_0^2 + h^2}},$$

where h is equal to one and half times the element size. Equation (6) is a first-order hyperbolic partial differential equation, which is solved using a positive-only upwinding scheme, described in [16]. Clearly, the characteristics of (6) point in the direction of $\mathbf{w}$. Therefore, for the points outside the drop $\mathbf{w}$ points away from the drop and for the points inside the drop it points inward. Thus, (6) can be solved by specifying the boundary condition $\phi = \phi_0$ at the two-fluid interface $\phi = 0$.

2.2. *Variation of Density, Viscosity, and Relaxation Time across the Interface*

In our finite-element scheme the fluid viscosity is assumed to take a jump across the interface; i.e.,

$$\eta = \begin{cases} \eta_d & \text{if } \phi < 0, \\ 0.5(\eta_d + \eta_L) & \text{if } \phi = 0, \\ \eta_L & \text{if } \phi > 0. \end{cases} \tag{7}$$

Here η_d and η_L are the viscosities of the fluids inside and outside the drop, respectively. In other words, the nodes that are inside the drop have the drop viscosity and those outside have the fluid viscosity. The fluid density, on the other hand, is assumed to vary smoothly across the interface

$$\rho = \begin{cases} \rho_d & \text{if } \phi < -h, \\ \rho_L & \text{if } \phi > h, \\ 0.5(\rho_d + \rho_L) + 0.5(\rho_d - \rho_L)\sin\left(\frac{\pi\phi}{2h}\right) & \text{otherwise,} \end{cases} \tag{8}$$

where h is equal to one and half times the element size, and ρ_d and ρ_L are the densities of the fluids inside and outside the drop, respectively. This smoothing of the density is similar to that in [2] and is needed for avoiding numerical instabilities for relatively large density ratios ρ_d/ρ_L. The fluid relaxation time is assumed to jump across the interface

$$\lambda_r = \begin{cases} \lambda_{rd} & \text{if } \phi < 0, \\ 0.5(\lambda_{rd} + \lambda_{rL}) & \text{if } \phi = 0, \\ \lambda_{rL} & \text{if } \phi > 0. \end{cases} \tag{9}$$

Here λ_{rd} and λ_{rL} are the relaxation times of the fluids inside and outside the drop, respectively. If the fluid inside (or outside) the drop is Newtonian, its relaxation time is set to zero. A relaxation time of zero ensures that the fluid relaxes instantaneously and thus behaves like a Newtonian fluid. This allows us to use the same equations for both Newtonian and viscoelastic liquids.

The surface-tension force is smoothed and acts only on the elements for which ϕ is smaller than h. This is done by approximating $\delta(\phi)$ in (2) with a mollified delta function $\delta_h(\phi)$ using the approach described in [2]:

$$\delta_h(\phi) = \begin{cases} \frac{(1+\cos(\pi\phi/h))}{2h} & \text{for } |\phi| < h, \\ 0 & \text{otherwise.} \end{cases}$$

We use an unstructured mesh for which the element size near the drop is kept approximately constant. This is used to define h to be one and half times the average element size near the drop, where the element size is equal to the side of a square whose area is two times that of a triangle.

The error introduced by smoothing the surface-tension force is $O(h)$ (see [22] for a detailed discussion). Also note that Eqs. (9) and (10) require that ϕ be maintained as a distance function, which we do in our implementation by reinitializing ϕ after each time step.

2.3. *Weak Form*

The weak form of the governing equations is obtained by multiplying Eqs. (1), (2), (4), and (5) by the test functions and integrating the second-order term by parts. Furthermore, since the fluid is viscoelastic, we also need to solve the constitutive equation (4) along with the momentum and continuity equations. In obtaining this weak form, the hydrodynamic stresses acting at the interface are completely eliminated.

To state the weak form for the equation of motion we need the spaces

$$
\begin{aligned}
W_u &= \{\mathbf{u} \in H^1(\Omega)^2 \mid \mathbf{u} = \mathbf{u}_\Gamma(t) \text{ on } \Gamma\},\\
W_{u0} &= \{\mathbf{v} \mid \mathbf{v} \in H^1(\Omega)^2 \text{ and } \mathbf{v} = 0 \text{ on } \Gamma\},\\
W_{\mathrm{A}} &= \{\mathbf{A} \in H^1(\Omega)^3 \mid \mathbf{A} = \mathbf{A}_{\mathrm{L}}(t) \text{ on } \Gamma^-\},\\
W_{\mathrm{A0}} &= \{\mathbf{A} \in H^1(\Omega)^3 \mid \mathbf{A} = 0 \text{ on } \Gamma^-\},\\
W_\phi &= \{\phi \in H^1(\Omega) \mid \phi = \phi_0(t) \text{ on } \Gamma^-\},\\
W_{\phi 0} &= \{\phi \in H^1(\Omega) \mid \phi = 0 \text{ on } \Gamma^-\},\\
L_0^2(\Omega) &= \left\{ q \in L^2(\Omega) \,\middle|\, \int_\Omega q \, d\mathbf{x} = 0 \right\},
\end{aligned}
\tag{10}
$$

where Γ^- is the upstream part of Γ. It is easy to show that the following weak formulation of the problem holds for the two-phase system:

For a.e. $t > 0$, find $\mathbf{u} \in W_u$, $\mathbf{A} \in W_{\mathrm{A}}$, $p \in L_0^2(\Omega)$, and $\phi \in W_\phi$, satisfying

$$
\int_\Omega \rho\left(\frac{d\mathbf{u}}{dt} - \mathbf{g}\right)\cdot \mathbf{v}\, d\mathbf{x} - \int_\Omega p\nabla\cdot\mathbf{v}\, d\mathbf{x} + \int_\Omega 2\eta_{\mathrm{s}}\mathbf{D}[\mathbf{u}] : \mathbf{D}[\mathbf{v}]\, d\mathbf{x} - \int_\Omega \mathbf{v}\cdot\nabla\cdot\left(\frac{c}{\lambda_{\mathrm{r}}}\mathbf{A}\right) d\mathbf{x}
$$

$$
- \int_\Omega \gamma\kappa\delta(\phi)\mathbf{n}\cdot\mathbf{v}\, d\mathbf{x} = 0 \quad \text{for all } \mathbf{v} \in W_{u0}, \tag{11}
$$

$$
\int_\Omega q\nabla\cdot\mathbf{u}\, d\mathbf{x} = 0 \quad \text{for all } q \in L^2(\Omega), \tag{12}
$$

$$
\mathbf{u}|_{t=0} = \mathbf{u}_{\mathrm{o}} \quad \text{in } \Omega, \tag{13}
$$

$$
\int_\Omega \left(\frac{\partial\mathbf{A}}{\partial t} + \mathbf{u}\cdot\nabla\mathbf{A} - \mathbf{A}\cdot\nabla\mathbf{u} - \nabla\mathbf{u}^T\cdot\mathbf{A} + \frac{1}{\lambda_{\mathrm{r}}}(\mathbf{A} - \mathbf{I})\right)\cdot\mathbf{s}\, d\mathbf{x} = 0 \quad \text{for all } \mathbf{s} \in W_{\mathrm{A0}}, \tag{14}
$$

$$
\mathbf{A}|_{t=0} = \mathbf{A}_{\mathrm{o}} \quad \text{in } \Omega, \tag{15}
$$

$$
\int_\Omega \left(\frac{\partial\phi}{\partial t} + \mathbf{u}\cdot\nabla\phi\right) g\, d\mathbf{x} = 0 \quad \text{for all } g \in W_{\phi 0}, \tag{16}
$$

$$
\phi|_{t=0} = \phi_0 \quad \text{in } \Omega.
$$

2.4. *Finite-Element Approximation*

In order to solve the above problem numerically, we discretize the domain using a finite-element triangulation T_h for the velocity and configuration tensor, where h is the mesh size, and a triangulation T_{2h} for the pressure. For approximating W_u, W_{u0},W_A, W_{A0}, $L^2(\Omega)$, $L_0^2(\Omega)$, W_ϕ, and $W_{\phi 0}$, the finite dimensional spaces are

$$\begin{aligned} W_{u,h} &= \{\mathbf{u}_h \in C^0(\bar{\Omega})^2 | \mathbf{v}_h|_T \in P_1 \times P_1 \text{ for all } T \in T_h, \mathbf{u}_h = \mathbf{u}_{\Gamma,h} \text{ on } \Gamma\}, \\ W_{0,h} &= \{\mathbf{v}_h \in C^0(\bar{\Omega})^2 | \mathbf{v}_h|_T \in P_1 \times P_1 \text{ for all } T \in T_h, \mathbf{v}_h = 0 \text{ on } \Gamma\}, \end{aligned} \tag{17}$$

$$\begin{aligned} L_h^2 &= \{q_h \in C^0(\bar{\Omega}) | q_h|_T \in P_1 \text{ for all } T \in T_{2h}\}, \\ L_{0,h}^2 &= \left\{ q_h \in L_h^2 \,\middle|\, \int_\Omega q_h \, d\mathbf{x} = 0 \right\}, \end{aligned} \tag{18}$$

$$W_{A,h} = \{\mathbf{s}_h \in C^0(\bar{\Omega})^3 | \mathbf{s}_h|_T \in P_1 \times P_1 \times P_1 \text{ for all } T \in T_h, \mathbf{s}_h = \mathbf{A}_{L,h} \text{ on } \Gamma^-\},$$

$$W_{A0,h} = \{\mathbf{s}_h \in C^0(\bar{\Omega})^3 | \mathbf{s}_h|_T \in P_1 \times P_1 \times P_1 \text{ for all } T \in T_h, \mathbf{s}_h = 0 \text{ on } \Gamma^-\}, \tag{19}$$

$$W_{\phi,h}^n = \{g_h \in H^1(\Omega) | g_h|_T \in P_1 \text{ for all } T \in T_h, g_h = \phi^n \text{ on } \Gamma^-\},$$

$$W_{\phi 0,h} = \{g_h \in H^1(\Omega) | g_h|_T \in P_1 \text{ for all } T \in T_h, g_h = 0 \text{ on } \Gamma^-\}, \tag{20}$$

$$W_{\phi R,h} = \{g_h \in H^1(\Omega) | g_h|_T \in P_1 \text{ for all } T \in T_h, g_h = 0 \text{ on the interface}\}. \tag{21}$$

Using these finite dimensional spaces, it is straightforward to discretize Eqs. (11)–(16). Notice that the discrete space $W_{\phi,h}$ assumes that ϕ is known on the upstream portion of the boundary. This is not a problem even when $\phi(t)$ is not known on the upstream boundary in advance because the imposed boundary value can be corrected during the reinitialization step. We remind the reader that since only the zero level set of $\phi(t)$ is physically relevant, as noted in [21], "we have a lot of freedom in treating $\phi(t)$ away from the interface." In our code, the value from the previous time step is used as the boundary value. Also note that the reinitialization space $W_{\phi R,h}$ assumes that ϕ remains zero along the interface, which is done by imposing a Dirichlet boundary condition, $\phi = 0$, along the interface during reinitialization iterations.

2.5. *Time Discretization Using the Marchuk–Yanenko Operator-Splitting Scheme*

The initial value problem (11)–(16) is solved by using the Marchuk–Yanenko operator-splitting scheme. This allows us to decouple its four primary difficulties: (i) the incompressibility condition and the related unknown pressure p_h; (ii) the nonlinear convection term; (iii) the interface problem and the related unknown level-set distribution ϕ_h; and (iv) the equation for the configuration tensor, and the viscoelastic stress tensor, which appears in the momentum equation.

The Marchuk–Yanenko operator-splitting scheme can be applied to an initial value problem of the form

$$\frac{d\phi}{dt} + A_1(\phi) + A_2(\phi) + A_3(\phi) + A_4(\phi) = f,$$

where the operators A_1, A_2, A_3, and A_4 can be multiple-valued.

Let Δt be the time step, and α_1 and α_2 be two constants: $0 \le \alpha_1, \alpha_2 \le 1$, and $\alpha_1 + \alpha_2 = 1$. We use the following version of the Marchuk–Yanenko operator-splitting scheme to simulate

the motion of drops and bubbles in a viscoelastic fluid. Set

$$\mathbf{u}^0 = \mathbf{u}_{0,h}, \quad \mathbf{A}^0 = \mathbf{A}_{0,h}, \quad \text{and} \quad \phi^0 = \phi_{0,h}. \tag{22}$$

For $n = 0, 1, 2, \ldots$, assuming $\mathbf{u}^n$, $\mathbf{A}^n$, and ϕ^n are known, find the values for $n+1$ using the following.

Step 1. Find $\mathbf{u}^{n+1/4} \in W_{u,h}$ and $p^{n+1/4} \in L^2_{0,h}$ by solving

$$\begin{aligned}\int_\Omega \rho \frac{\mathbf{u}^{n+1/4} - \mathbf{u}^n}{\Delta t} \cdot \mathbf{v}\, d\mathbf{x} - \int_\Omega p^{n+1/4} \nabla \cdot \mathbf{v}\, d\mathbf{x} + \alpha_1 \int_\Omega 2\eta_s \mathbf{D}\big[\mathbf{u}^{n+1/4}\big] : \mathbf{D}[\mathbf{v}]\, d\mathbf{x} \\ = \int_\Omega \mathbf{v} \cdot \nabla \cdot \left(\frac{c}{\lambda_r}\mathbf{A}^n\right) d\mathbf{x} + \int_\Omega \gamma \kappa \delta(\phi)\mathbf{n} \cdot \mathbf{v}\, d\mathbf{x} \quad \text{for all } \mathbf{v} \in W_{0,h},\end{aligned}$$

$$\int_\Omega q \nabla \cdot \mathbf{u}^{n+1/4}\, d\mathbf{x} = 0 \quad \text{for all } q \in L^2_h. \tag{23}$$

Step 2. Find $\mathbf{u}^{n+2/4} \in W_{u,h}$ by solving

$$\begin{aligned}\int_\Omega \rho \frac{\mathbf{u}^{n+2/4} - \mathbf{u}^{n+1/4}}{\Delta t} \cdot \mathbf{v}\, d\mathbf{x} + \int_\Omega \rho_L\big(\mathbf{u}^{n+2/4} \cdot \nabla \mathbf{u}^{n+2/4}\big) \cdot \mathbf{v}\, d\mathbf{x} \\ + \alpha_2 \int_\Omega 2\eta_s \mathbf{D}\big[\mathbf{u}^{n+2/4}\big] : \mathbf{D}[\mathbf{v}]\, d\mathbf{x} = 0 \quad \text{for all } \mathbf{v} \in W_{0,h}.\end{aligned} \tag{24}$$

Step 3. Find $\mathbf{A}^{n+3/4} \in W_{A,h}$ by solving

$$\begin{aligned}\int_\Omega \Bigg(\frac{\mathbf{A}^{n+3/4} - \mathbf{A}^n}{\Delta t} + \mathbf{u}^{n+2/4} \cdot \nabla \mathbf{A}^{n+3/4} - \mathbf{A}^{n+3/4} \cdot \nabla \mathbf{u}^{n+2/4} - \big(\nabla \mathbf{u}^{n+2/4}\big)^T \cdot \mathbf{A}^{n+3/4} \\ + \frac{1}{\lambda_r}\big(\mathbf{A}^{n+3/4} - \mathbf{I}\big)\Bigg) \cdot \mathbf{s}\, d\mathbf{x} = 0 \quad \text{for all } \mathbf{s} \in W_{A0,h}.\end{aligned} \tag{25}$$

Step 4. Find $\phi^{n+4/4} \in W^n_{\phi,h}$ by solving

$$\int_\Omega \left(\frac{\phi^{n+4/4} - \phi^n}{\Delta t} + \mathbf{u}^{n+2/4} \cdot \nabla \phi^{n+4/4} \right) g_h\, d\mathbf{x} = 0 \quad \text{for all } g_h \in W_{\phi 0,h}. \tag{26}$$

Set $\mathbf{u}^{n+1} = \mathbf{u}^{n+2/4}$, $\mathbf{A}^{n+1} = \mathbf{A}^{n+3/4}$, $p^{n+1} = p^{n+1/4}$, $\phi^{n+1} = \phi^{n+4/4}$.

Step 5. Reinitialize ϕ^{n+1}. Set $\phi^0_R = \phi^{n+1}$. For $r = 0, 1, 2, \ldots$,

$$\mathbf{w}^r = S(\phi^{n+1}) \frac{\nabla \phi^r_R}{\big|\nabla \phi^r_R\big|}.$$

Find $\phi^{r+1}_R \in W_{\phi R,h}$ by solving

$$\int_\Omega \left(\frac{\phi^{r+1}_R - \phi^r_R}{\Delta t} + \mathbf{w}^r \cdot \nabla \phi^r_R \right) g_h\, d\mathbf{x} = \int_\Omega S(\phi^{n+1})\, g_h\, d\mathbf{x} \quad \text{for all } g_h \in W_{\phi R,h}. \tag{27}$$

Go back to the above for loop.

Set $\phi^{n+1} = \phi^{r+1}_R$ and go back to the first step.

Remarks

1. The first step gives rise to a Stokes-like problem for the velocity and pressure distributions which is solved by using a CG method [16].

2. The second step is a nonlinear problem for the velocity, which is solved by using a least-squares CG algorithm [17].

3. The third step is a linearized hyperbolic problem for the configuration tensor or stress. This problem is solved by using a third-order upwinded positive-only scheme [18]. The two key features of this scheme are a positive-only scheme that guarantees that the configuration tensor remains positive definite, and a third-order upwinding scheme for discretizing the advection term in the constitutive equation. These two features are important for obtaining a scheme that is stable at relatively large De numbers.

4. In this paper, we assume that $\alpha_1 = \alpha_2 = 0.5$.

5. The fourth step is a hyperbolic problem for the scalar level-set function ϕ. This problem is solved by using a upwinding scheme where the advection term is discretized using a third-order scheme [18, 19, 23]. That is, $\mathbf{u} \cdot \nabla\phi$ at $\mathbf{x}^0$ is estimated using the known values of ϕ at the five points $\mathbf{x}^{-2}$, $\mathbf{x}^{-1}$, $\mathbf{x}^0$, $\mathbf{x}^1$, and $\mathbf{x}^2$, which lie on the line that is parallel to $\mathbf{u}$ and passes through $\mathbf{x}^0$,

$$\mathbf{u} \cdot \nabla\phi(\mathbf{x}^0) = |\mathbf{u}(\mathbf{x}^0)| \sum_j \frac{\tau_j \phi(\mathbf{x}^j)}{h}.$$

The points $\mathbf{x}^{-2}$ and $\mathbf{x}^{-1}$ are upstream points, and $\mathbf{x}^1$ and $\mathbf{x}^2$ are downstream points. Here distance $h = |\mathbf{x}^{-1} - \mathbf{x}^0|$ and

$$\tau_i = \frac{\prod_{i \neq 0, j}(\xi^0 - \xi^j + \alpha)}{\prod_{i \neq j}(\xi^i - \xi^j)} \quad \text{for } i \neq 0,$$

$$\tau_0 = -\sum_{i \neq 0} \tau_i,$$

where $\xi^i = |\mathbf{x}^i - \mathbf{x}^0|/h$. For $\alpha = 0$ the above approximation is centered and fourth-order accurate, and for $\alpha > 0$ it is upwinded and third-order accurate. The degree of upwinding is controlled by α; in our simulations, we use $\alpha = 3$ which was picked by trial and error.

6. After advecting ϕ, we reinitialize ϕ to be a distance function near the interface by performing two iterations of (27). It is important to note that the surface $\phi(t) = 0$ does not change during reinitialization. This is done by first determining the elements that contain a $\phi(t) = 0$ surface and then forming a list of the nodes that are on these elements. The task of keeping a $\phi(t) = 0$ surface fixed during the reinitialization step is equivalent to keeping $\phi(t)$ fixed for these nodes, which can be done by applying the Dirichlet boundary condition. The space used in (27) for simulations is therefore a smaller subspace of space $W_{\phi R,h}$ defined in (21).

3. NUMERICAL RESULTS

We next discuss the numerical results obtained using the above algorithm for the deformation/motion of drops and bubbles in Newtonian and Oldroyd-B liquids. The parameter c in the Oldroyd-B model is assumed to be one (i.e., $\eta_s = \eta_p$). We also assume that all

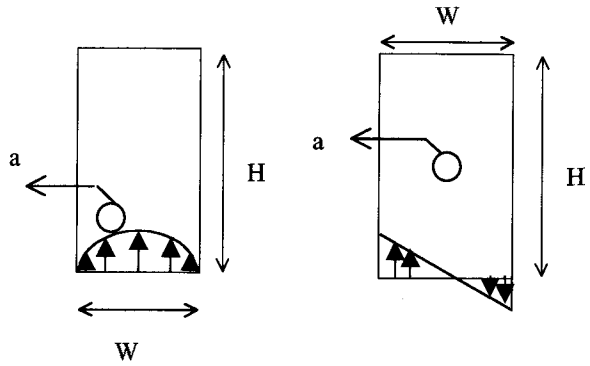

FIG. 1. Typical computational domains with sides W and H used in our simulations. In the first figure, the drop is subjected to a pressure-driven flow and in the second to a simple shear flow. In both cases, the velocity distribution is prescribed on the domain boundary.

dimensional quantities are in centimeter–gram–second units. Parameters such as surface tension, applied shear rate, viscosity ratio, and density difference are varied to demonstrate that the numerical method can be used to efficiently compute interface problems for a wide range of these parameters.

We discuss results for the following three cases: deformation of drops under shear flows, deformation of Newtonian drops in pressure-driven viscoelastic flows, and deformation of Newtonian bubbles rising in quiescent Newtonian and viscoelastic liquids. For the case of drops subjected to simple shear flows we consider cases where the drop is viscoelastic and the fluid is Newtonian, and vice versa.

Simulations are performed in a rectangular-shaped domain with sides W and H, as shown in Fig. 1. For simple shear flow studies, an initially circular drop is placed at the center of the domain and subjected to a simple shear flow by moving the left and right walls of the domain in opposite directions. The density ratio in these simulations is assumed to be one. In the bubble-rise studies, an initially circular bubble placed near the bottom of the domain rises, as it is lighter than the surrounding liquid. In pressure-driven flows, a circular drop is placed near the left-hand bottom corner of the computational domain. The flow at the domain inlet is assumed to be parabolic. In all simulations, the initial state of the configuration tensor is assumed to be

$$\mathbf{A}_0 = \mathbf{I}.$$

The initial value $\mathbf{A}_0 = \mathbf{I}$ implies that the Oldroyd-B fluid is in a relaxed state.

3.1. *Convergence with Mesh Refinement*

The code was verified by performing a convergence study that shows that the steady state shape of the drop is independent of the mesh resolution and also of the time step used in the calculations. A typical unstructured mesh with a relatively finer resolution near the drop surface used in these simulations is shown in Fig. 2. The time step was varied between 0.001 and 0.0005.

Simulations are started by placing a circular drop of diameter 1 at $t = 0$ at the center of the computational domain, where it is subjected to a viscoelastic simple shear flow of strength 0.4 s^{-1}. The domain sides are $W = 5$ and $H = 10$. The fluid viscosity is 300 and

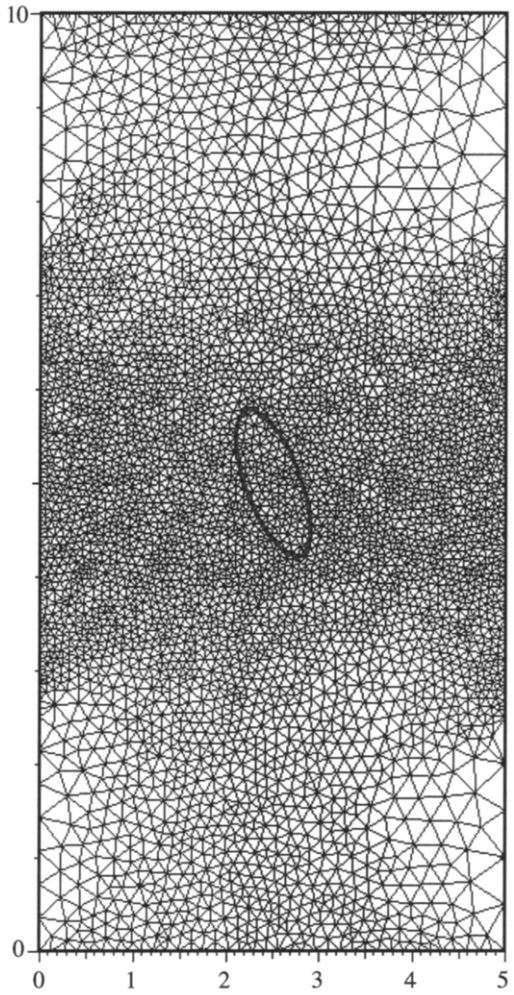

FIG. 2. A typical finite-element mesh used for the simple shear flow problems and the deformed drop shape are shown. The parameters are the same as in Fig. 4. The pressure elements are shown. Note that there is a higher concentration of nodes around the center of the domain where the drop is placed. The mesh contains 8394 elements, 4305 pressure nodes, and 17,003 velocity nodes.

$\lambda = 1$. The relaxation time of the fluid is 1, and the surface tension is 250. For the above parameters, $\mathrm{Re} = 0.0003$, $\mathrm{De} = 0.4$, and $\mathrm{Ca} = 0.24$. As we discuss later, for these parameter values the drop attains a steady state shape.

From Table I we note that when the number of nodes is increased from 9129 to 11,567, and further to 17,493, the steady state deformations as well as the drop areas are comparable. The drop area for the finest mesh is $\sim$1.5% smaller than the initial area. The mesh was refined such that in all three cases the elements near the interface were four times smaller than the elements farther away. For a mesh with 17,493 nodes the drop area and deformation are shown in Table II for two different values of the time step. From this table we note that the steady state results are also approximately independent of the time step. The time evolution curves of the drop shape shown in Fig. 3 for two different values of time step and mesh resolution are also approximately identical. We may therefore conclude that both the transient and the steady state solutions are independent of the mesh resolution and the time step used.

TABLE I

Drop Deformation and Area for Three Different Mesh Resolutions for a Newtonian Drop Subjected to a Simple Shear Flow

No. of nodes	Deformation D	Drop area
9,129	0.4758	0.7387
11,567	0.4863	0.7327
17,493	0.4779	0.7694

Note. The time-step size is 0.0001. Ca = 0.24, Re = 0.0003, and De = 0.4.

For the simple shear flow problems discussed in this and the next sections, we were able to successfully simulate flows up to De = 16 using a mesh with 11,576 nodes for which the element size near the drop is ~0.09. The method converges for Re < O(1000), including Stokes flow (Re = 0). The Reynolds number for most cases described in this paper is much smaller than one and is approximately of the same order as for experiments described in [24].

The qualitative nature of trA distribution shown in Figs. 4a–4c also remains approximately the same when the mesh resolution is increased and when the time step is decreased. From these figures we note that the maximum value of trA is near the tip of the major axis of the deformed drop. Also note that the viscoelastic stress distribution, and consequently also the drop deformation, is not symmetric about the drop major axis. In other words, the deformed drop is not exactly of an elliptical shape. This result is in agreement with experiments that show that the drops and bubbles in viscoelastic flows do not deform to symmetric shapes, unless the flow itself is symmetric [20]. In fact, even when the flow is symmetric the drop shape may not be symmetric (e.g., a bubble rising in a viscoelastic liquid may develop a two-dimensional cusp-shaped trailing edge). This implies that fully three-dimensional simulations are needed for understanding these asymmetrical deformations of viscoelastic drops subjected to simple shear flows.

3.2. *Deformation of a Newtonian Drop in a Simple Shear Flow of a Viscoelastic Liquid*

We next consider the case of a Newtonian drop subjected to a simple shear flow of a viscoelastic liquid. The initial drop diameter is 1 and the shear rate is 0.4 s^{-1}. The fluid viscosity is 300 and $\lambda = 1$. The Reynolds number is 0.0003.

TABLE II

Drop Deformation and Area for Two Different Values of Time Step for a Newtonian Drop Subjected to a Simple Shear Flow

Time step	Deformation D	Drop area
0.0005	0.4749	0.7659
0.001	0.4779	0.7694

Note. The number of nodes is 17,493. Ca = 0.24, Re = 0.0003, and De = 0.4.

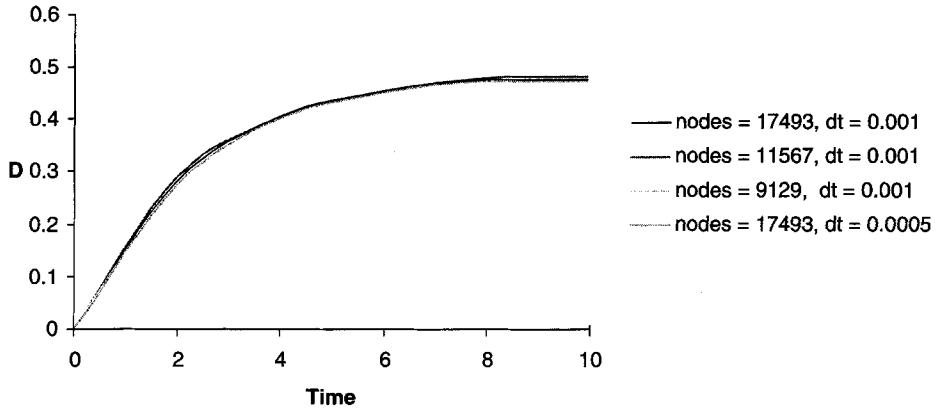

FIG. 3. Transient deformation of a Newtonian drop in a viscoelastic shear flow for Ca = 0.24, De = 0.4, and Re = 0.0003. The drop attains a stable, approximately elliptical shape. The figure shows that for varying resolution and time steps, the final deformations as well as transient deformations are approximately the same.

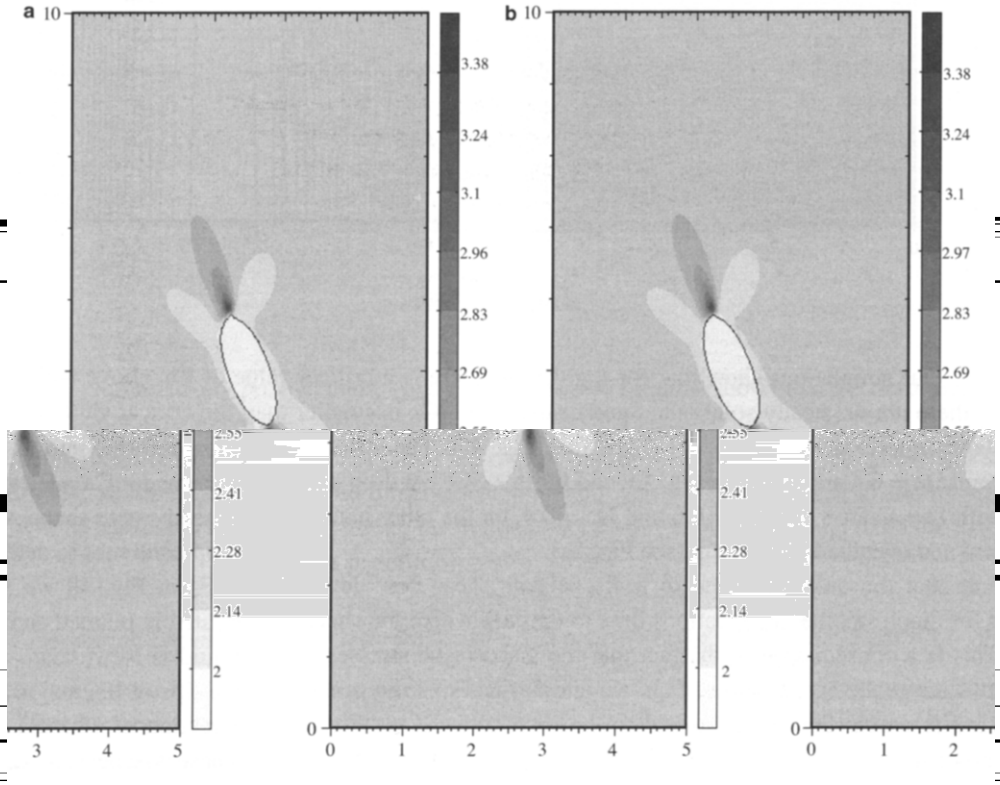

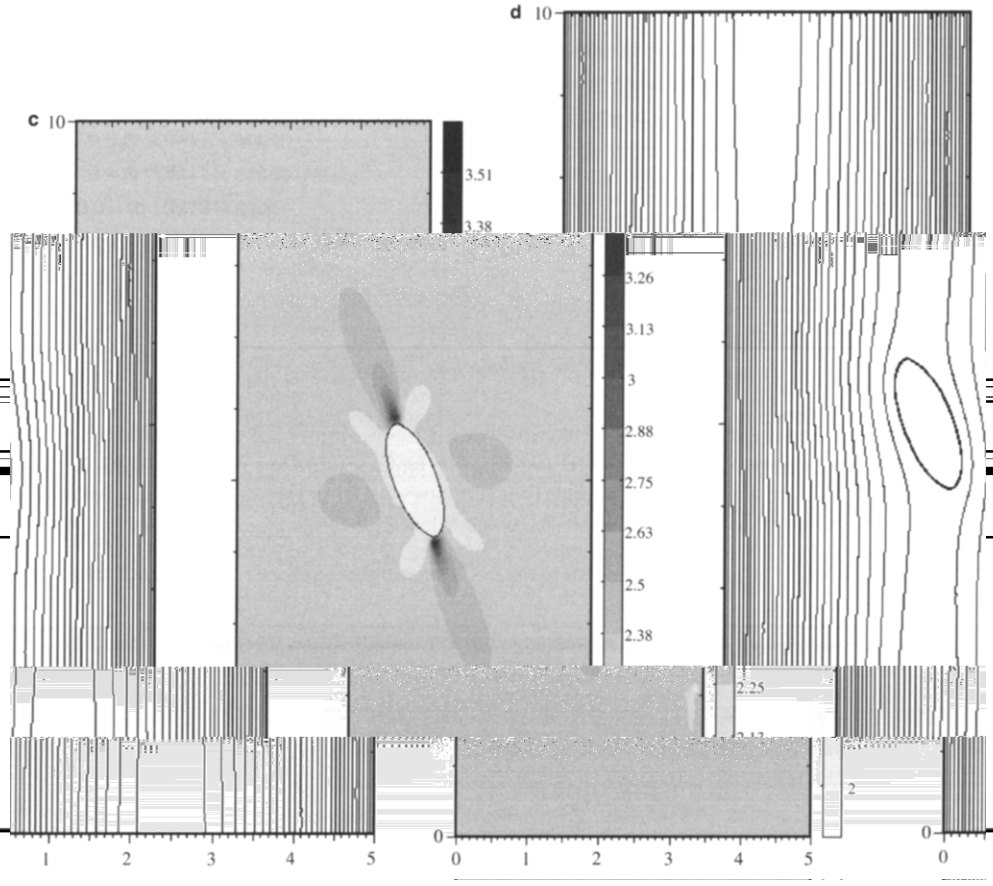
c
d
10
3.51
3.38
3.26
3.13
3
2.88
2.75
2.63
2.5
2.38
2.25
2
0
1
2
3
4
5

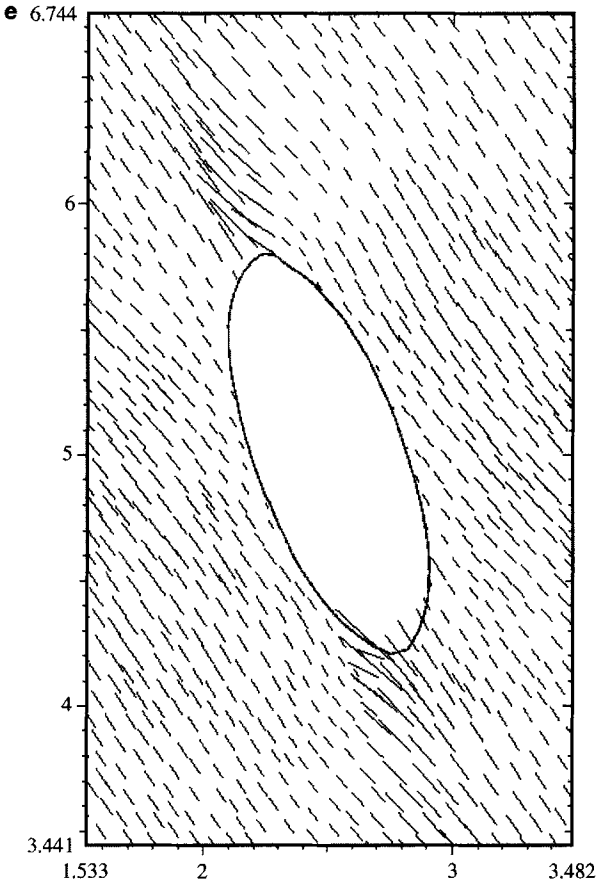

FIG. 4—*Continued*

to develop relatively pointed ends. Analysis of the cross sections shows that the deformed drop is not axisymmetric.

In this paper we restrict ourselves to presenting the numerical scheme. Further results of three-dimensional simulations as well as the breakup and tip streaming, which require much higher resolution to accurately capture breaking from the tips, will be addressed in a future paper [26].

3.3. *Deformation of a Viscoelastic Drop in a Simple Shear Flow of a Newtonian Liquid*

Next, we describe the behavior of a viscoelastic drop subjected to a simple shear flow of a Newtonian liquid. The drop diameter is 1 and the shear rate 0.4 s^{-1}. The fluid viscosity is 300 and $\lambda = 1$. The Reynolds number is 0.0016. Our focus is to investigate the role of De and Ca on the drop deformation. In our simulations De and Ca are varied independently by changing the relaxation time of the fluid inside the drop and the surface tension.

As is the case for a Newtonian drop, for a fixed De the deformation increases with increasing Ca. From Fig. 6a we note that for $Ca = 0.6$ and $De = 0.4$ the viscoelastic drop is not significantly deformed (i.e., $D = 0.4675$). From this figure we also note that the distribution of trA is not symmetrical about the major axis and that the maximum value of trA is near the tip of the approximate major axis. The thin boundary layers inside the drop

where trA is relatively large are, however, not symmetrically located about the major axis (see Figs. 6a and 7). Due to this asymmetry of viscoelastic stresses the deformed drop is not exactly symmetric about the major axis. For Ca = 60 and De = 8.0, at $t = 10$ the drop is significantly deformed, with $D = 0.8152$, as shown in Fig. 7. For these parameter values the drop does not reach a steady state shape and continues to deform. The maximum value of trA in this case is not near the tip of the major axis.

From Fig. 6b we note that the viscoelastic stresses inside the drop are extensional near the major axis tips, as the principal direction of the configuration tensor near the tips is approximately normal to the drop surface. From Fig. 8a we note that for a constant value of Ca, the maximum value of trA increases with increasing De. The extensional viscoelastic stresses pull the drop surface inward near the ends of the major axis, and therefore the drop deformation decreases when De is increased. This trend, however, reverses for the higher values of De, for which the drop deformation increases with increasing De (see Fig. 8b).

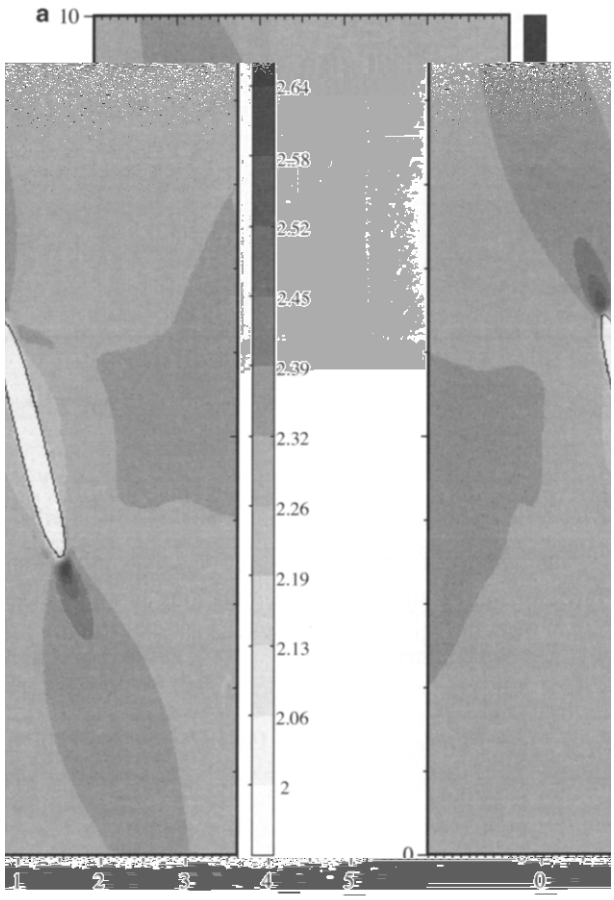

FIG. 5. (a) A Newtonian drop subjected to a viscoelastic shear flow for De = 0.4, Ca = 0.6, Re = 0.0003 and time step = 0.001. At $t = 10$, deformation $D = 0.8402$. For these parameter values, the drop continues to deform and eventually breaks up. Isovalues of trA at $t = 10$ are shown. Notice that trA and thus viscoelastic stresses are higher near the tips along the major axis of the drop. (b) Deformation of a three-dimensional Newtonian drop subjected to a viscoelastic simple shear flow in the xz-plane. The velocity field imposed on the boundary is independent of y. The number of nodes is 136,161, De = 0.1, Ca = 0.3, and the time step = 0.0003. At $t = 0.9$, deformation $D = 0.1502$. (c) The parameters are the same as in (b). At $t = 2.1$, deformation $D = 0.5624$.

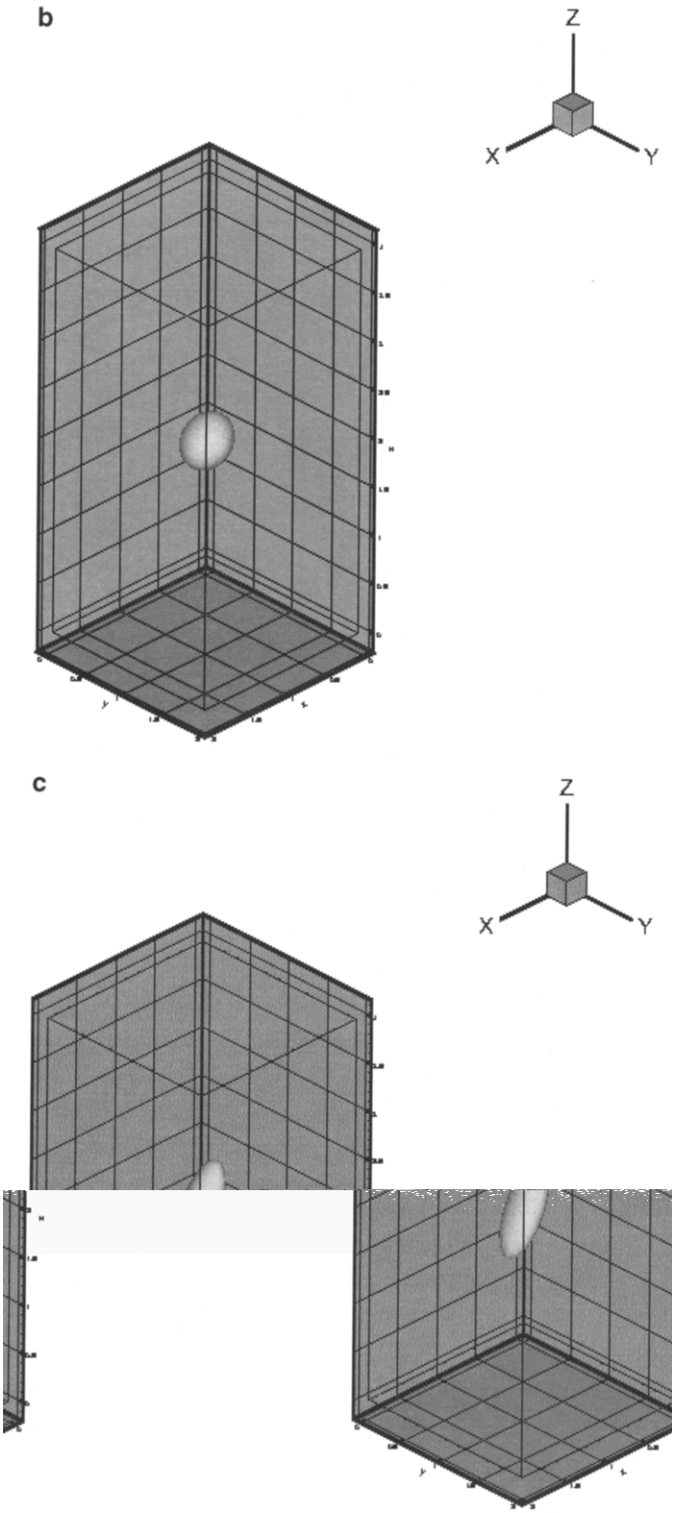

FIG. 5—*Continued*

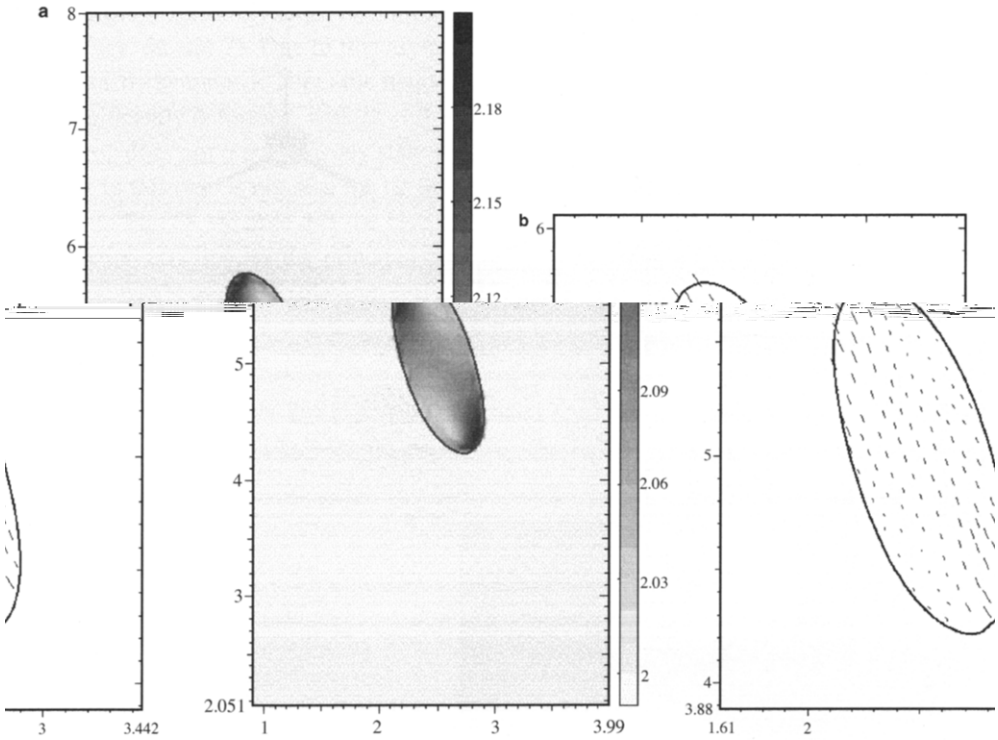

FIG. 6. (a) A magnified view of isovalues of tr**A** is shown for a steady state viscoelastic drop in a simple shear flow of a Newtonian fluid. Notice that tr**A** is relatively large near the tips along the major axis of the drop and that the distribution of tr**A** is not symmetric about the approximate major axis. The stress boundary layer, the thin region where tr**A** is relatively large, is not symmetrically located about the major axis. The time step used is 0.001. For Ca = 0.6, De = 0.4, and Re = 0.0003, steady state deformation $D = 0.4675$. (b) A magnified view of the distribution of the principal direction of **A** is shown for the case described in (a). Notice that near the major axis tips the principal direction of the configuration tensor is approximately normal to the drop surface.

This behavior of viscoelastic liquids is not unexpected. For example, the drag coefficient for a cylinder placed in an Oldroyd-B fluid decreases with De for De $< \sim$O(1). But, for the higher values of De the drag coefficient increases with increasing De. This is a consequence of the memory, and resulting nonlinearly, of the Oldroyd-B fluid. It was suggested in [9] that this reversal of trend at higher De is due to the modification of the velocity field from that for a Newtonian liquid. Specifically, at higher De, the shear rate in the region where the polymer stretch is relatively large is smaller than that for a Newtonian fluid in the same flow geometry.

Also notice that in Fig. 7 the elongated drop is not small compared to the domain size, and thus the obtained results are not independent of the computational domain size. But since in this paper our main goal is to present the numerical method, we simply note that a larger sized domain should be used to make these results independent of the domain size.

3.4. *Newtonian Drops in Pressure-Driven Viscoelastic Flows*

Next, we describe the results for the case where a Newtonian drop is placed in a pressure-driven flow of a viscoelastic liquid. This problem is of interest in many material processing applications where polymer blends are subjected to pressure-driven flows. The flow causes

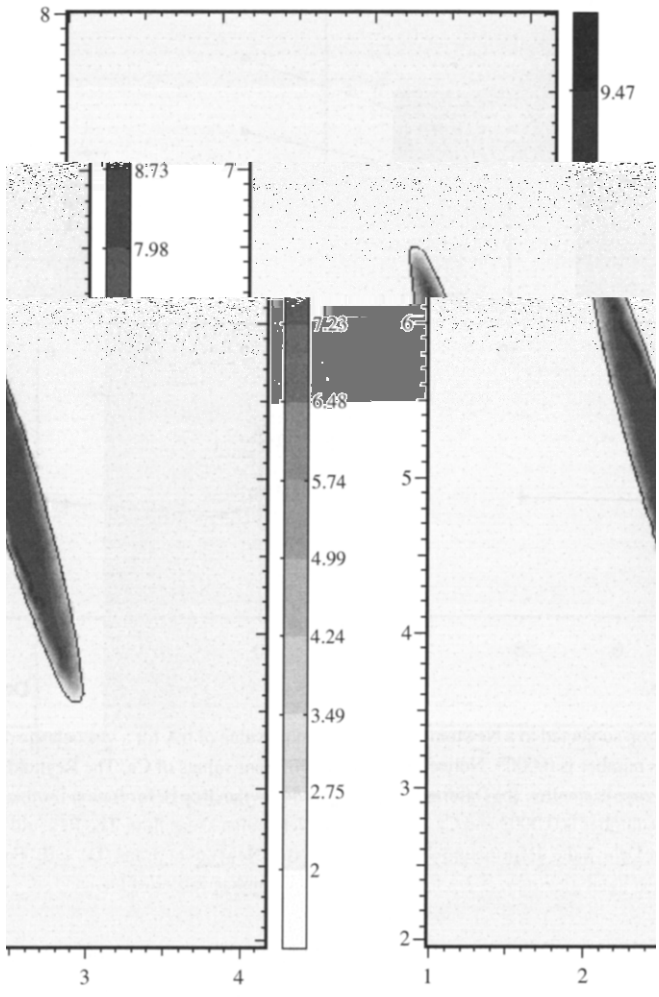

FIG. 7. A viscoelastic drop in a simple shear flow of a Newtonian fluid for Ca = 60, De = 8.0, and Re = 0.0003. The time step is 0.001. The results are shown at $t = 10$. Deformation $D = 0.8152$. The drop breaks up in this case. A magnified view of isovalues of tr**A** is shown. Notice that the maximum value of tr**A** is not near the tips.

the droplets in an immiscible polymer blend to stretch and break up, which leads to mixing. Our goal here is to study the drop deformation as it moves through the domain.

The domain is rectangular with sides measuring 7 and 4. The flow at the bottom of the domain is assumed to be parabolic, with a centerline velocity of 1. A drop with an initial diameter of 1 is placed at $x = -3$ and $y = -6$. The fluid viscosity is 200, $\lambda = 1$. The dimensionless parameters based on the centerline velocity are De = 5, Ca = 2000, and Re = 0.005.

Our simulation shows that the drop stretches and orients, as shown in Fig. 9a. The interesting feature of deformation is that the front of the drop is relatively round but the trailing edge becomes sharper and assumes a cusp-like shape at high De, as shown in Fig. 9a. In a simple shear flow the principal direction of stretch is at 45° to the flow direction, and so the drop is stretched along this direction. From this figure we note that the front of the drop is closer to the channel centerlines and hence its velocity is larger than that of the trailing edge, which is closer to the channel wall. Therefore, the drop, as it moves upward in

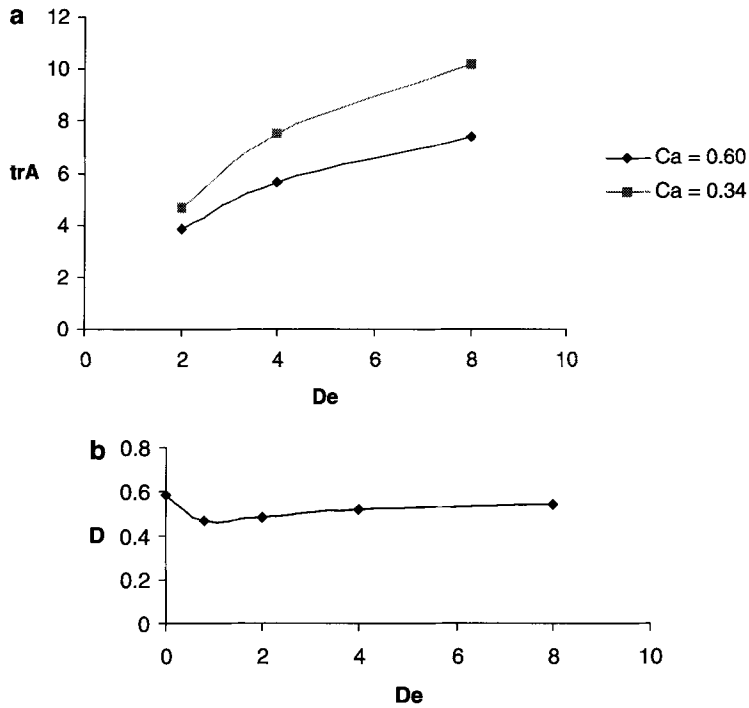

FIG. 8. (a) The maximum value of trA for a viscoelastic drop subjected to a Newtonian shear flow is shown as a function of De, for two different values of Ca. The Reynolds number is 0.0003. Notice that the maximum value of trA is larger for Ca = 0.34, as the drop deformation for this case is smaller. (b) Deformation as a function of De for a viscoelastic drop in Newtonian shear flow. The Reynolds number is 0.0003 and Ca = 0.6. Viscoelastic drops are less deformed compared to Newtonian drops (De = 0). For De < 1 the deformation decreases with increase in De, but this trend reverses for higher values of De.

the pressure-driven flow, also rotates in the counterclockwise direction and bends such that the center of curvature of the lower surface moves to the outside [25]. This bending of the drop gives the impression that it is rotating in the clockwise direction even though, as noted above, the rotation is in the counterclockwise direction. Another interesting feature of the drop deformation at $t = 3.9$ is that the center of curvature of the lower surface is outside the drop. From Fig. 9b we also note that trA is relatively large near the cusp-shaped trailing edge, and we may therefore conclude that the viscoelastic stresses cause the formation of a sharp trailing edge.

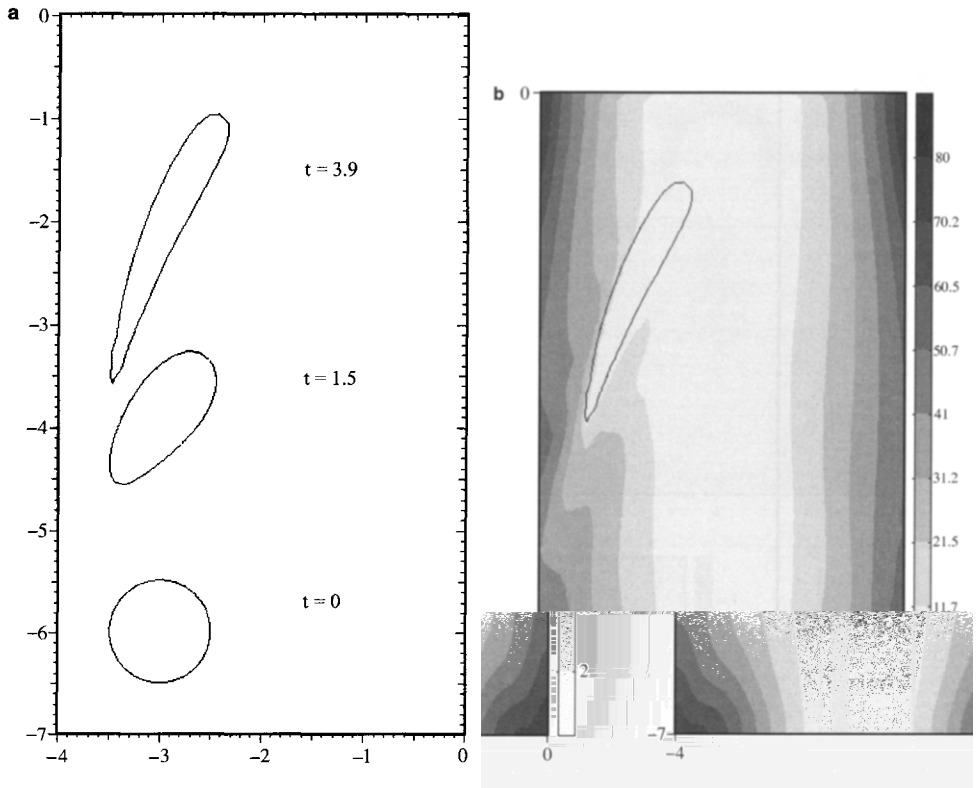

FIG. 9. A Newtonian drop in a viscoelastic pressure-driven flow. The density ratio is 1, $\lambda = 1$, De = 5, Ca = 2000, Re = 0.005, and the time step = 0.001. (a) The time-dependent shapes at $t = 0$, 1.5 and 3.9 are shown. Notice that at $t = 3.9$, the front of the drop is relatively round and the trailing edge is sharp. (b) At $t = 3.9$ isovalues of trA are shown. Notice that trA is relatively large near the cusp-shaped trailing edge.

velocity,

$$V_b = \frac{\int_{\phi \le 0} v \, dA}{A_d},$$

where $\phi \le 0$ defines the area occupied by the drop, $A_d = \int_{\phi \le 0} dA$ is the drop area, and v is the y-component of velocity inside the drop.

As expected, when an initially circular bubble is released in a liquid of larger density it starts to accelerate upward because of the buoyancy force. The mass-averaged bubble velocity first increases rapidly with time and then changes slowly with time, but it does not reach a constant value, as the bubble shape continues to change with time. The bubble velocity in the latter time interval can be considered approximately constant. For calculating Re and De we have used the approximately constant value of V_b.

In Fig. 10 the time evolution of the shape of a bubble rising in a Newtonian liquid is shown. The viscosity ratio is 1 and the density ratio is 5. The Reynolds number is 0.d136 and Ca is 2.272. From Fig. 10 we note that at $t = 0.25$ the bubble trailing edge begins to move inward and the local center of curvature moves to the outside of the bubble. At $t = 0.45$ the bubble deforms to an umbrella-like shape. The bubble shape remains symmetrical about the vertical, passing through the center for all times. We note that for the smaller values of Ca,

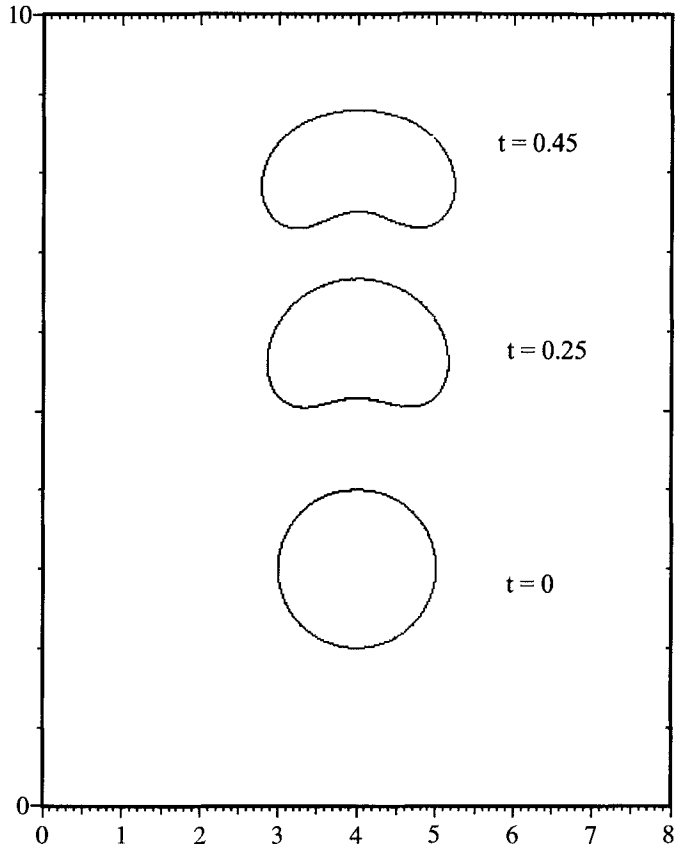

FIG. 10. The shape of a Newtonian bubble rising in a Newtonian fluid is shown at $t = 0$, 0.25 and 0.45. The time step is 0.0005. The density ratio is 5 and λ is 1. The area-averaged velocity at $t = 0.25$ is 11.36. Based on this velocity Re = 0.1136 and Ca = 2.272.

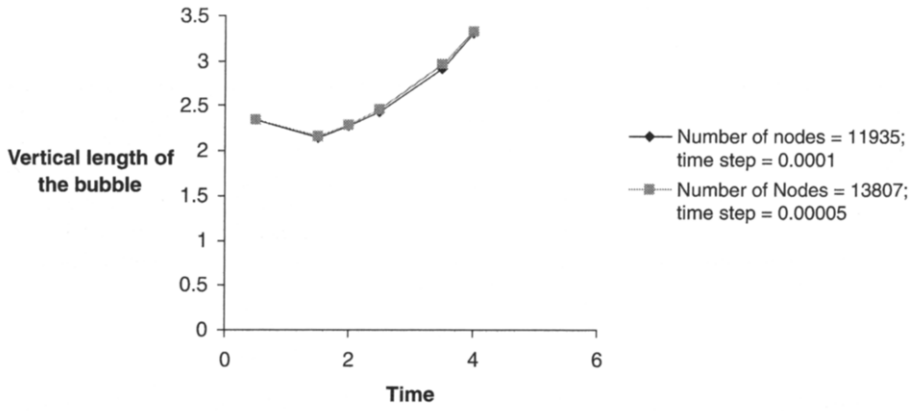

FIG. 11. The vertical dimension of a Newtonian bubble rising in an Oldroyd-B fluid is shown as a function of time. The density ratio = 5, $\lambda = 1$, Ca = 21.6, De = 1.62, and Re = 0.01. For varying resolution and time steps, the transient deformations are approximately the same.

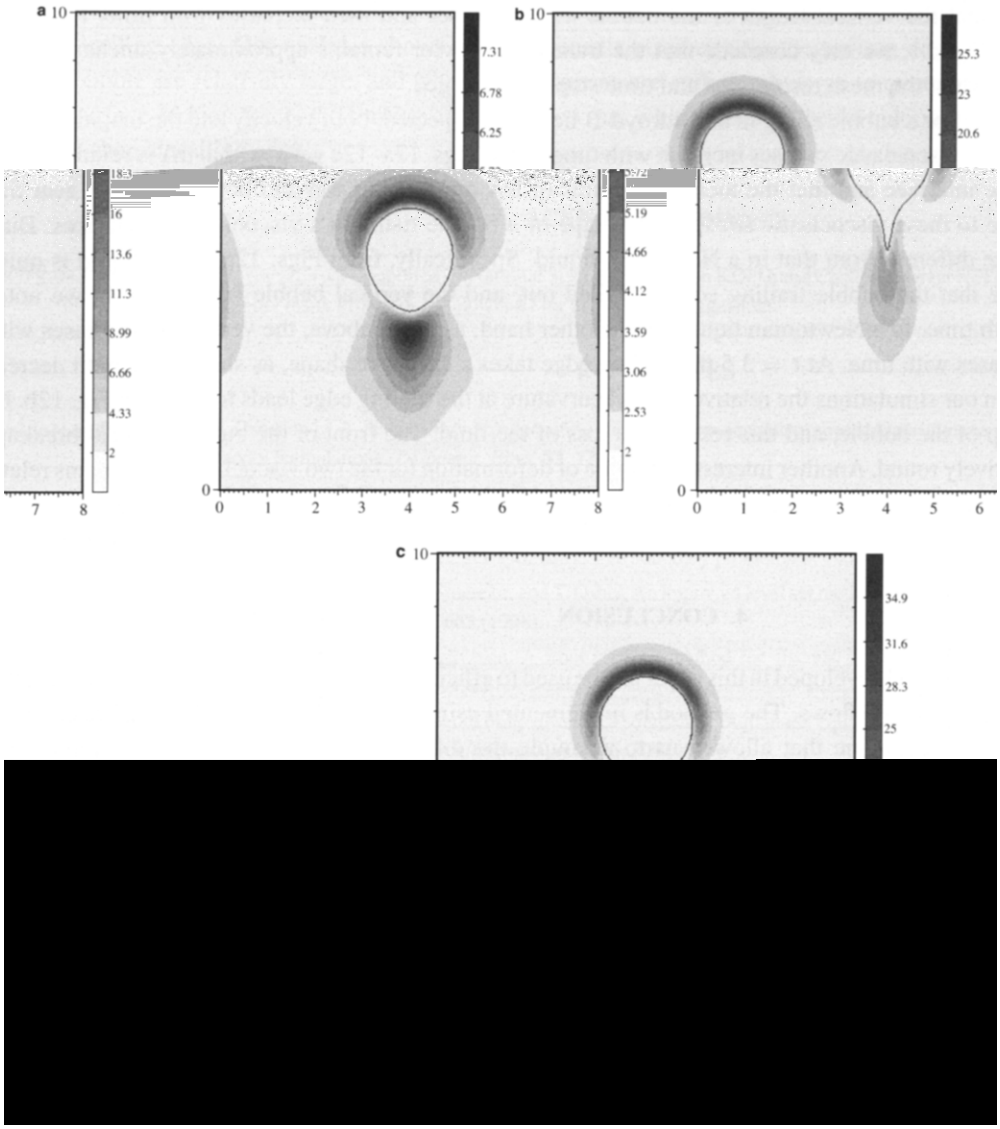

FIG. 12. Isovalues of trA are shown for a buoyancy-driven Newtonian drop rising in the Oldroyd-B fluid for the density ratio of 5, $\lambda = 1$, and time step of 0.0001. (a) At $t = 1.5$ the area averaged velocity is 1.08, and based on this velocity, Re = 0.01, Ca = 21.6, and De = 1.62. (b) At $t = 3.5$, the area-averaged velocity is 0.84, and based on this velocity, Re = 0.0084, De = 1.261, and Ca = 16.81. Note that the viscoelastic stresses are relatively large near the interface and cause the formation of a characteristic cusp-like trailing edge. (c) Isovalues of trA are shown for a Newtonian drop rising in the Oldroyd-B fluid for a density ratio of 10, $\lambda = 10$, and time step = 0.0001. Notice that the relatively large values of viscoelastic stresses near the interface cause the formation of the characteristic cusp-like trailing edge. At $t = 1.4$, the area-averaged velocity is 2.15, and based on this velocity, Re = 0.0215, Ca = 4.3, and De = 3.225.

the bubble rising in a Newtonian liquid remains approximately circular and symmetrical about the vertical.

The time evolutions of the shapes of rising bubbles in the Oldroyd-B liquid are shown in Fig. 11 for two different values of resolution and time step. For this bubble, $\rho = 1$, density ratio = 5, $\eta_L = 200$, $\lambda = 1$, Re = 0.01, De = 1.62, and Ca = 21.6. From this figure we note

that the vertical length of the bubble first decreases and then increases with time. From Fig. 11, we may conclude that the transient behavior remains approximately unchanged when the mesh resolutions and time steps are changed.

For a bubble rising in an Oldroyd-B liquid, as expected, both velocity and the magnitude of viscoelastic stresses increase with time. From Figs. 12a–12c we note that tr**A** is relatively large near the interface and that the local maximums of tr**A** are near the top and bottom surfaces. Due to these viscoelastic stresses, the shape of a bubble rising in a viscoelastic liquid is quite different from that in a Newtonian liquid. Specifically, from Figs. 12a and 12b, we note that the bubble trailing edge is pulled out, and the vertical bubble length increases with time. In a Newtonian liquid, on the other hand, as noted above, the vertical length decreases with time. At $t = 3.5$ the trailing edge takes a cusp-like shape, as shown in Fig. 12b. In our simulations the relatively small curvature at the trailing edge leads to the local breakup of the bubble, and this results in a loss of the fluid. The front of the bubble remains relatively round. Another interesting feature of deformation for the two viscoelastic cases is that for $\mathrm{Ca} = 4.3$, the drop shape is prolate (see Fig. 12b), but for $\mathrm{Ca} = 21.6$ it is oblate (see Fig. 12c).

4. CONCLUSION

The level-set method developed in this paper can be used to efficiently compute the motion of viscoelastic two-phase flows. The method is implemented using the Marchuk–Yanenko operator-splitting technique that allowed us to decouple the difficulties associated with the incompressibility constraint, the nonlinear convection and viscoelastic terms, and the interface problem. The linear systems for resulting subproblems are solved using schemes that do not require assembly of the global matrix. The constitutive equation is solved using a scheme that uses a third-order upwind discretization for the advection term and guarantees the positive definiteness of the configuration tensor. To validate our numerical method, we have studied the deformation of drops in simple shear flows, and the deformation and motion of rising bubbles, over a wide range of dimensionless capillary and Deborah numbers. We have verified that the results are independent of the mesh resolution as well as the size of the time step.

Our simulations for $\lambda = 1$ show that when a Newtonian drop is subjected to a viscoelastic simple shear flow, there is a critical value of Ca above which there are no steady solutions. Similarly, for a viscoelastic drop subjected to a simple shear flow of a Newtonian liquid for a given De, there is a maximum value of Ca for which the drop attains a steady state shape. It is interesting to note that for the viscoelastic drop in a shear flow of Newtonian fluid, when $\mathrm{De} < \sim O(1)$ the drop deformation is smaller than that for a Newtonian drop at the same Ca value because the viscoelastic stresses inside the drop tend to reduce deformation. The opposite is true for a Newtonian drop placed in a viscoelastic shear flow, as the viscoelastic stresses of the bulk fluid tend to increase drop deformation. In fact, in this case the radius of curvature near the tips is significantly smaller, which leads to tip streaming. A Newtonian drop placed in a pressure-driven viscoelastic flow deforms such that its front remains relatively round but the trailing edge assumes a cusp-like shape.

Simulations show that a Newtonian bubble rising in a Newtonian liquid assumes an umbrella-like shape. A Newtonian bubble rising in a viscoelastic liquid, on the other hand, assumes an elongated shape and for some parameter values the trailing edge assumes a cusp-like shape. These results are in agreement with the experimental observations

reported in [20], where the authors observed the formation of a two-dimensional cusp-like trailing edge. Our analysis shows that viscoelastic stresses near the trailing edge of the bubble are relatively large, and when these stresses are sufficiently large to overcome the surface-tension force, the trailing edge is pulled out, which leads to the formation of a cusp-shaped trailing edge.

ACKNOWLEDGMENTS

This research was supported by National Science Foundation KDI Grand Challenge Grant NSF/CTS-98-73236. The authors thank Professor R. Glowinski for his valuable suggestions.

REFERENCES

1. S. Osher and J. A. Sethian, Fronts propagating with curvature-dependent speed: Algorithms based on Hamilton-Jacobi formulations, *J. Comput. Phys.* **83**, 12 (1988).
2. M. Sussman, P. Smereka, and S. Osher, A level set approach for computing solutions to incompressible two-phase flow, *J. Comput. Phys.* **114**, 146 (1994).
3. M. Sussman and P. Smereka, Axisymmetric free boundary problems, *J. Fluid Mech.* **341**, 269 (1997).
4. M. Sussman, E. Fatemi, P. Smereka, and S. Osher, An improved level set method for incompressible two-phase flows, *Comput. Fluids* **27**, 663 (1998).
5. S. O. Unverdi and G. Tryggvason, A front-tracking method for viscous, incompressible, multifluid flows, *J. Comput. Phys.* **100**, 25 (1992).
6. E. Fatemi and F. Odeh, Upwind finite difference solution of Boltzmann equation applied to electron transport in semiconductor devices, *J. Comput. Phys.* **108**, 209 (1993).
7. C. W. Hirt and B. D. Nichols, Volume of fluid (VOF) methods for the dynamics of free boundaries, *J. Comput. Phys.* **39**, 201 (1981).
8. G. Ryskin and L. G. Leal, Numerical solution of free-boundary problems in fluid mechanics. Part 1. The finite-difference technique, *J. Fluid Mech.* **148**, 1 (1984).
9. D. W. Bousfield, R. Keunings, and M. M Denn, Transient deformation of an inviscid inclusion in a viscoelastic extensional flow, *J. Non-Newtonian Fluid Mech.* **27**, 205 (1988).
10. D. S. Noh, I. S. Kang, and L. G. Leal, Numerical solutions for the deformation of a bubble rising in a dilute polymeric fluids, *Phys. Fluids* **5**(6), 1315 (1993).
11. S. Ramaswamy and L. G. Leal, The deformation of a viscoelastic drop subjected to steady uniaxial extensional flow of a Newtonian fluid, *J. Non-Newtonian Fluid Mech.* **85**, 127 (1999).
12. S. Ramaswamy and L. G. Leal, The deformation of a Newtonian drop in the uniaxial extensional flow of a viscoelastic liquid, *J. Non-Newtonian Fluid Mech.* **88**, 149 (1999).
13. G. I. Marchuk, Splitting and alternate direction methods, in *Handbook of Numerical Analysis*, edited by P. G. Ciarlet and J. L. Lions, North-Holland, (Amsterdam, 1990), Vol. 1, 197–462.
14. R. Glowinski, T. W. Pan, T. I. Hesla, and D. D. Joseph, A distributed Lagrange multiplier/fictitious domain method for particulate flows, *Int. J. Multiphase Flows* **25**(5), 755 (1999).
15. P. Singh, D. D. Joseph, T. I. Hesla, R. Glowinski, and T. W. Pan, A distributed Lagrange multiplier/fictitious domain method for viscoelastic particulate flows, *J. Non-Newtonian Fluid Mech.* **91**, 165 (2000).
16. R. Glowinski, P. Tallec, M. Ravachol, and V. Tsikkinis, Chap. 7 in *Finite Elements in Fluids*, edited by T. J. Chung (Hemisphere, Washington DC, 1992), Vol. 8.
17. M. O. Bristeau, R. Glowinski, and J. Periaux, Numerical methods for Navier–Stokes equations. Application to the simulation of compressible and incompressible flows, *Comput. Phys. Rep.* **6**, 73 (1987).
18. P. Singh and L. G. Leal, Finite element simulation of the start-up problem for a viscoelastic fluid in an eccentric rotating cylinder geometry using a third-order accurate upwind scheme, *Theor. Comput. Fluid Mech.* **5**, 107 (1993).
19. R. Glowinski and O. Pironneau, Finite element methods for Navier–Stokes equations, *Annu. Rev. Fluid Mech.* **24**, 167 (1992).

20. Y. J. Liu, T. Y. Liao, and D. D. Joseph, A two-dimensional cusp at the trailing edge of an air bubble rising in a viscoelastic liquid, *J. Fluid Mech.* **304**, 321 (1995).
21. Y. C. Chang, T. Y. Hou, B. Merriman, and S. Osher, A level set formulation of Eulerian interface capturing methods for incompressible fluid flows, *J. Comput. Phys.* **124**, 449 (1996).
22. J. U. Brackbill, D. B. Kothe, and C. Zemach, A continuum method for modelling surface tension, *J. Comput. Phys.* **100**, 335 (1992).
23. M. Tabata and S. Fujima, An upwind finite element scheme for high Reynolds number flows. *Int. J. Numer. Methods Fluids* **14**, 305 (1991).
24. W. J. Milliken and L. G. Leal, Deformation and breakup of viscoelastic drops in planar extensional flows, *J. Non-Newtonian Fluid Mech.* **40**, 355 (1991).
25. S. K. Dey, C. Jacob, and M. Xanthos, Inert-gas extrusion of rigid PVC foam, *Annu. Tech. Conf. ANTEC* **V3**(3), 4138 (1995).
26. S. B. Pillapakkam, P. Singh, and L. G. Leal, Direct numerical simulations of deformation drops and bubbles in viscoelastic flows using the level-set method, manuscript in preparation.